Design of a Hydrogen-Powered Crashworthy eVTOL Using Multidisciplinary Analysis and Design Optimization

Keijzer, D.M.; Simon Soria, C.; Arends, J.J.; Sarıgöl, B.; Scarano, F.; Castro, Saullo G.P.

DOI
10.2514/6.2024-2474

Publication date
2024

Document Version
Final published version

Published in
Proceedings of the AIAA SCITECH 2024 Forum

10.2514/6.2024-2474

Design of a Hydrogen-Powered Crashworthy eVTOL Using Multidisciplinary Analysis and Design Optimization

Damien Keijzer
Faculty of Aerospace Engineering, Delft University of Technology, 2629 HS Delft, Netherlands

Carmelo Simón Soria
ISAE-SUPAERO, 31400 Toulouse, France

Jorick Arends, Barkın Sarıgöl, Fulvio Scarano, Saullo G.P. Castro*
Faculty of Aerospace Engineering, Delft University of Technology, 2629 HS Delft, Netherlands

As of present the Urban Air Mobility market has been dominated by fully electric aircraft. However, hydrogen vehicles have remained relatively undeveloped in this segment, also because hydrogen poses additional design complexities and uncertainties concerning crashworthiness, fuel cell cooling, and low volumetric density. Nevertheless, hydrogen might yield advantages in mission performance owing to its superior gravimetric energy density and greater sustainability when compared to batteries. In this paper, the design procedure of a four-passenger long-range hydrogen eVTOL using Multidisciplinary Analysis and Design Optimization (MADO) is presented. Using MADO, the mission energy of the eVTOL was minimized while abiding by the constraints rooting from the use of hydrogen. Based on this design, the conclusion can be made that the implementation of hydrogen eVTOLs in urban air mobility is feasible whilst taking into account constraints resulting from the use of hydrogen at the preliminary design stage. This led to an aircraft which excels at longer range due to the increased scalability of hydrogen fuel, but having a weight penalty due to auxiliary equipment which hampers its performance and results in a large fuselage and maximum takeoff weight.

I. Nomenclature

eVTOL	=	electric Vertical Takeoff or Landing
UAM	=	Urban Air Mobility
VTOL	=	Vertical Takeoff and Landing
TRL	=	Technology Readiness Level
EOM	=	Equations of Motion
MADO	=	Multidisciplinary Analysis and Design Optimization

l_{fuse}	=	Length of fuselage
w_{fuse}	=	Width of fuselage
ϕ_f	=	Perimeter of fuselage
ϵ	=	Downwash
α	=	angle of attack
Γ	=	dihedral
M	=	mass
t_{r_h}	=	T
AR	=	Aspect ratio
b	=	Span
E	=	Energy
sp	=	Specific

II. Introduction

VTOL aircraft are not a revolutionary concept, military vehicles have used VTOL capabilities for several decades. However, until recently this technology has remained exclusive to military applications, helicopters and small-scale multicopters. In the past decade, advancements have been made towards the application of this technology to UAM (Urban Air Mobility) vehicles, destined to transport civilians within, or between cities in a rapid, efficient manner using air-borne vehicles. These vehicles are categorised in short-, medium-, and long-range vehicles. The latter representing the segment of UAM vehicles with a range beyond approximately 200 km, enough to fly between different cities.

*Corresponding author, email: S.G.P.Castro@tudelft.nl

Copyright © 2024 by Delft University of Technology, Faculty of Aerospace Engineering.
Published by the American Institute of Aeronautics and Astronautics, Inc., with permission.

The development of these vehicles has focused on the use of electrical power, to comply with environmental development plans such as the Paris 2015 agreement, making these VTOL aircraft to be renamed as electric-VTOL, or eVTOL. Meanwhile, major aircraft manufacturers have turned their attention towards the use of hydrogen for long-range combustion-powered aircraft, as it poses an easily adaptable solution to reducing the carbon emissions by air-borne vehicles. The difference in power source selection comes from developing a new product versus adapting an existing and well-functioning product. The interest of using electrical power comes from the batteries' high power density, although their low gravimetric energy density tampers the possibilities of exploring long-range applications due to a rapid increase of weight. Hydrogen has a high gravimetric energy density, approximately 3 times higher than kerosene or SAF [1], but the safety risks and its low volumetric energy density obstruct the development of this technology for aircraft.

The objective of this paper is thus to demonstrate the capabilities of hydrogen for long-range VTOL UAM vehicles, merging both development trends of eVTOL UAM vehicles and use of hydrogen in civilian aircraft, by presenting a novel design methodology. The design encounters significant technical and regulatory challenges, being the regulatory challenges originated from the application of hydrogen systems in civilian air transport, which has not been widely explored yet and may entail a risk of explosion. The technical challenges are mainly driven by the low power delivered by hydrogen fuel cells, and the need for more advanced thermo-management systems. Furthermore, the high volume required to store hydrogen and convert it to electricity also showed to be a challenging factor, especially when crashworthiness aspects are considered.

It is for this reason that, for a sample design named "Aetheria", the MADO framework, the developed sub-systems, and its key design and performance parameters are presented in the present study. We display the methods used to perform a preliminary design of a crashworthy, hydrogen powered long-range VTOL UAM vehicle, as well as to assure its feasibility.

III. Design Baseline

The preliminary design outlined in this paper aligns with the high-level requirements portrayed in Table 1. The rationale behind these requirements is detailed in the technical report[2], where a comprehensive range and market analysis has been conducted. The user requirements enumerated in Table 1 generate a substantial amount of system and subsystem requirements. As this paper offers a condensed overview, the complete list of requirements is left for the reader in [2]. It is important to note that the labels assigned to the requirements here may not directly correspond to those specified in the technical report.

Table 1 Summary of user requirements

Label	Description
VTOL-USER-01	The UAM vehicle shall be VTOL capable.
VTOL-USER-02	The UAM vehicle shall be able to fly 400 km.
VTOL-USER-03	The UAM vehicle shall be able to fly at a cruise speed of 300 [km/h].
VTOL-USER-04	The UAM vehicle shall be able to carry a payload of 510 kg (1 pilot + 4 passengers).
VTOL-USER-05	The aircraft shall be compliant with 'Survivable Emergency Landing' crashworthiness conditions specified in EASA MOC SC-VTOL[3].
VTOL-USER-06	The aircraft shall weigh less than 3175 [kg].
VTOL-USER-06	The aircraft shall be hydrogen powered.

Following the requirements in Table 1, a configuration was selected as the baseline for the multidisciplinary analysis and design optimization process. The trade-off and rationale for this specific configuration are detailed in [4]. The chosen configuration is visually represented in Figure 1. Notably, a crucial characteristic of this design involves the attachment of two engines to each propeller. This setup ensures that even in the event of an engine failure, 50% of the total shaft power remains accessible, meeting stringent controllability demands in more extreme scenarios. The underlying assumption relies on the propeller's resilience against catastrophic failure due to a bird-strike during hovering. This assumption is grounded in the rarity of birds colliding with quasi-stationary objects.

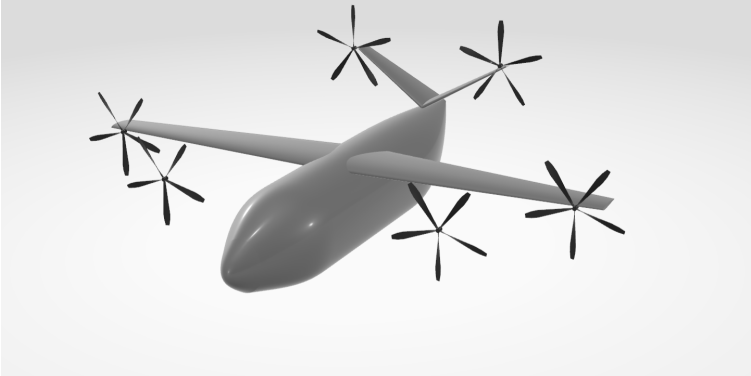

Fig. 1 Preliminary sketch illustrating the initial configuration, serving as the foundation for the MADO framework.

IV. System Modelling

Before the definition of the MADO problem, the modelling of each subsystem will be elaborated on. Each system will then be integrated according to the MADO definition described in section V. The design has been divided into the following subsystems: aerodynamics & performance, stability and control, power, propulsion, and structures.

A. Aerodynamics & Performance

The wing planform is sized assuming a trapezoidal wing. Performance requirements are derived from maximum climb rate and gradient, stall speed, maximum speed and turning performance. These performance metrics are then used to find the design point for the wing- and power- loading. The geometry of the wing planform can be computed using a pre-defined value for the aspect ratio (A). The taper ratio is fixed at 0.45 such that a nearly elliptical lift distribution could be achieved.

The airfoil of the wing is selected through a trade off, by the simplification of choosing a single airfoil along the span of the wing. This resulted in the selection of the NACA2412, because of its large drag bucket and high $C_{l,max}$. The details of the trade-off are left out for conciseness but are to be found in [5].

Translating the airfoil performance to a finite wing is done with the method specified in [6]. DeYoung and Harper introduced a methodology to assess the lift distribution across wings featuring diverse characteristics like arbitrary sweep, twist, taper, and lower aspect ratios. Using this method, C_{L_α} and the lift-induced component of the drag polar can be computed.

In order to find the zero lift drag, a component drag estimation is performed. The method is defined by Equation 1, as found in [7], where the equations for the individual components are to be found.

$$C_{D_0} = \frac{1}{S_{ref}} \sum C_{f_e} \cdot FF_c \cdot IF_c \cdot S_{wet_c} + C_{D_{misc}} \tag{1}$$

The zero lift drag can then be added to the induced drag to compute the drag polar. An aspect which this model lacks is the $C_{L_{max}}$ estimation, which is defined only in the initial estimate. The implications of this are discussed in the section V and recommendations are made in section VIII.

To estimate the energy consumption of the aircraft for a nominal mission, the assumptions listed in Table 2 are made. The transition from vertical flight to horizontal and vice-versa is not modelled, as the added complexity has no contribution to the fidelity of the estimation. This assumption is based on the work performed in [8], where the transition had been modeled for a tandem wing aircraft.

Table 2 Assumptions used for estimating the energy of the aircraft for a nominal mission.

Label	Assumptions
TRANS-01	The transition phase has a negligible energy consumption and is accounted for by a safety factor of 20% increase in energy from the vertical climb phase.
CLIMB-01	The aircraft climbs at a gradient of 0.065 [-].
CLIMB-02	The aircraft climbs at the optimal lift coefficient and its corresponding velocity.
DESCENT-01	The aircraft descends with its engines set to zero thrust (feathered) and follows the glide slope.

Using these assumptions, the energy consumed by the aircraft could be deduced using the basic equations of motion (EOM) of the aircraft as listed in [9]. The analysed phases are split into climb, cruise, descend, horizontal/vertical loiter and vertical flight. An essential procedure involves converting the calculated thrust requirement into power, a step facilitated by Equation 2, which transforms thrust values into their corresponding power equivalents.

$$P_a = T \cdot V + 1.2 \cdot T \cdot \left(-\frac{V}{2} + \sqrt{\frac{V^2}{4} + \frac{T}{2\rho \cdot A_{\text{disk}}}} \right) \tag{2}$$

Let A_{disk} be the disk area, ρ the air density and V the speed of the eVTOL. Then, using Equation 2, an energy estimation on the various phases can be made.

- **Climb:** The climb is modeled by computing the optimal C_L, found by maximising $\frac{C_L^3}{C_D^2}$. From this, the required thrust can be readily found using the weight, climb speed and climb gradient listed in Table 2.
- **Cruise:** Modelling the cruise phase is performed by solving the equations of motion in steady flight. The thrust is then converted to power using Equation 2. Finally, the energy is found by multiplying the obtained power by the duration of the cruising phase.
- **Descent:** As from assumption DESCENT-01 in Table 2, the EOM are solved with no thrust force (feathered), corresponding to a gliding descent. The energy consumption is therefore assumed to be negligible.
- **Loitering:** Loitering for an eVTOL is an important part of its concept of operations. Hence, it must be taken into account for the energy consumption. In horizontal flight configuration, a 20 minutes loiter is performed at the minimum drag speed. In vertical flight configuration, it is assumed to be performed exclusively in case of emergencies, when no other option is available. Hence, the duration is based on the time it would take to cover the distance from transition altitude to the helipad. The rationale being that in this time another VTOL experiencing an emergency could land with priority.
- **Vertical flight and transition:** The energy for the vertical flight phase is modeled through the calculating the energy required to rise at constant rate of 2 m/s using equation (2). Then transition is taken into account by increasing the energy consumption from the vertical climb by 20%.

Adding up the various phases, the total mission energy can be computed and utilized to size the power system.

B. Stability and Control

The stability and controllability of the aircraft exhibits itself with certain conditions in the MADO. In terms of horizontal flight stability and control, the aircraft must satisfy the requirements specified in Table 3. As per Roskam, a design value of $C_{n_\beta} = 0.0571$ is selected[10].

Table 3 Requirements for a stable and controllable aircraft in horizontal flight

Condition	Direction	Requirement	Limiting case
Stable	Longitudinally	$C_{m_\alpha} < 0$	Cruise condition
	Laterally	$C_{n_\beta} > 0$	V_s
Controllable	Longitudinally	$C_m = 0$	Horizontal landing
	Laterally	Certified for landing in cross-wind of $0.2V_s$[11] and roll rate $p \geq 60°/1.3s$[12]	Horizontal landing, V_s

In addition to the displayed ones, there are other requirements in terms of stability and controllability. Stability augmentation systems (SASs) are designed to further damp the horizontal flight eigenmodes. The SASs are developed independently of the MADO and, since these systems do not drive the aircraft geometry design, they are not discussed further in this paper. Additionally, the pylon sizing (for the wing-mounted, inward propellers) is done independently and validated to produce a functional design.

1. Stability and Control Optimization For Horizontal Flight

The empennage configuration of the aircraft must be selected before the MADO process. Given that the design baseline specifies the implementation of a high-wing design, only a T-tail or a V-tail are reasonable empennage options to avoid wake interference. Since the design baseline envisions tail-mounted propellers, a V-tail is developed to reduce structural complexity and vibrations.

A lower level optimization process inside the greater MADO process is performed to determine the necessary parameters for the overall optimisation. The stability and control optimization methodology is shown below for a V-tail, designed from a separate virtual horizontal and vertical tail.

For each wing position with respect to the fuselage $\bar{x}_{wing}$, corresponds a minimum empennage surface area for which the stability and control boundaries are satisfied. This is found by performing a scissor plot for each wing location by applying Equation 3 and Equation 4[7], and determining the minimum empennage area. This is however dependent on the tail's aspect ratio. A loop is performed over a range of empennage aspect ratios, and the smallest empennage is chosen that satisfies the geometrical constraints dictated by propeller-propeller and propeller-fuselage clearances (for tail-mounted propellers).

$$\frac{S_h}{S} = \frac{1}{\left(\frac{C_{L_{\alpha_h}}}{C_{L_{\alpha_{A-h}}}}\left(1 - \frac{d\epsilon}{d\alpha}\right)\frac{l_h}{\bar{c}}\left(\frac{V_h}{V}\right)^2\right)}\bar{x}_{cg} - \frac{\bar{x}_{ac} - S.M.}{\left(\frac{C_{L_{\alpha_h}}}{C_{L_{\alpha_{A-h}}}}\left(1 - \frac{d\epsilon}{d\alpha}\right)\frac{l_h}{\bar{c}}\left(\frac{V_h}{V}\right)^2\right)} \tag{3}$$

$$\frac{S_h}{S} = \frac{1}{\frac{C_{L_h}}{C_{L_{A-h}}}\frac{l_h}{\bar{c}}\left(\frac{V_h}{V}\right)^2}\bar{x}_{cg} + \frac{\frac{C_{m_{ac}}}{C_{L_{A-h}}} - \bar{x}_{ac}}{\frac{C_{L_h}}{C_{L_{A-h}}}\frac{l_h}{\bar{c}}\left(\frac{V_h}{V}\right)^2} \tag{4}$$

In the equations above, $\frac{S_h}{S}$ is the ratio of the virtual horizontal tail area to the main wing area, $C_{L_{\alpha_h}}$ is the horizontal tail's lift gradient, $C_{L_{\alpha_{A-h}}}$ is the aircraft-less-tail's lift gradient, $\frac{d\epsilon}{d\alpha}$ is the downwash coefficient, l_h is the distance between the wing's aerodynamic center and the tail's aerodynamic center, $\bar{c}$ is the MAC length, $\frac{V_h}{V}$ is the ratio of velocities over the tail to over the wing, $\bar{x}_{cg}$ is the limiting case CG location normalised with respect to the MAC (0 is the MAC leading edge, 1 is the MAC trailing edge), $\bar{x}_{ac}$ is the aerodynamic center's location normalised with respect to the MAC, $S.M.$ is an industry standard safety margin of 0.05, C_{L_h} is the tail's lift coefficient during landing (limiting case), $C_{L_{A-h}}$ is the aircraft-less-tail's lift coefficient during landing (limiting case), and $C_{m_{ac}}$ is the wing's moment coefficient at the aerodynamic center.

In order to size the virtual vertical tail, the design value of $C_{n_\beta} = 0.0571$ is enforced by taking the contributions of the virtual vertical tail and the fuselage. By applying estimation methods derived from [13][14][15], the virtual vertical tail's surface area can be determined to follow Equation 5.

$$S_v = \frac{C_{n_{\beta_{req}}} - \frac{-2 \cdot V_{fus}}{Sb}}{K C_{L_{\alpha_{V_N}}}} \cdot \frac{Sb}{l_v} \qquad K = 0.1035 ln\left(A_V\right) + 0.5618 \tag{5}$$

In this equation, S_v corresponds to the area of the virtual vertical tail, $C_{n_{\beta_{req}}}$ is the design value of C_{n_β}, V_{fus} is the fuselage external volume, S is the main wing's surface area, b is the wingspan, $C_{L_{\alpha_{V_N}}}$ is the normal-to-V-tail lift gradient, l_v is the distance from the wing's aerodynamic center to the V-tail's aerodynamic center, and A_V is the V-tail's aspect ratio. The term $\frac{-2 \cdot V_{fus}}{Sb}$ corresponds to the fuselage's contribution to C_{n_β}[15].

The design parameters of the V-tail follow after the determination of the areas of the virtual horizontal and vertical tail. Equation 6 is used to determine the V-tail's surface area and dihedral angle S_{vee} and Γ_{vee}[14].

$$S_{vee} = S_h + S_v \qquad \Gamma_{vee} = \arctan\left(\sqrt{\frac{S_v}{S_h}}\right) \tag{6}$$

The ailerons and ruddervators are designed to satisfy the requirements on roll rate p, $C_{n_{\delta r}}$ during cross-wind landing, and $C_{m_{\delta e}}$ for elevator effectiveness. The ruddervators combine the latter two requirements as they act both as an elevator and a rudder. The ruddervators have a specified maximum deflection angle of $\delta_{re} = \pm 20°$, and the ailerons have a specified maximum deflection angle of $\delta_a = \pm 30°$, as suggested in literature[13][14]. The designed variable for the ruddervators is the control surface chord to V-tail chord ratio, with a fixed control surface span to be equal to that of the V-tail, as is common in aircraft with V-tail empennages. However, the designed variable for the ailerons is the span of the control surface from the wingtip, with a fixed control surface chord to wing chord ratio of 0.25, common value for aircraft.

2. Stability and Control Optimization For Vertical Flight

In order to assess the stability and controllability of the aircraft in vertical flight, the present eVTOL design is treated to be essentially a hexacopter. In order to verify the controllability, the ACAI toolbox is used[16]. The Available Control Authority Index determines whether a multicopter is controllable and to what extent, given by the index of its controllability, under given circumstances and aircraft characteristics.

The variables are, amongst others, the CG location on the projection plane, the location of the rotors on the projection plane, the external forces acting on the aircraft, and the available maximum thrust per rotor. For each calculation involving the ACAI method, the following conditions have been taken into account, to ensure redundancy and safety for the passengers and any person or object in the vicinity of a vertical flight manoeuvre. As per CS-27 requirements[17], the aircraft must remain controllable under a vertical wind gust of 9.1m/s, and a lateral cross-wind of 31km/h without compromising flight safety. Additionally, a single-engine-failure scenario is envisioned for all calculations. As previously stated, each propeller is powered by two engines, so a single-engine-failure will reduce the maximum thrust on its propeller to half the nominal value. The most stringent case of these failures in each case is used for the design.

By finding the CG locations in which the ACAI changes sign, the vertical flight mode CG range can be determined. In order to ensure flight safety, this range should at least cover the CG range defined by the static loading diagram.

The wing-mounted, inward-propellers' pylon sizing, which is performed independently of the MADO, is found by a compromise between the propulsion department and the structural department. A shorter pylon reduces its structural complexity, with the cost of a less cruise-efficient propeller that can deliver a higher maximum thrust. However, a longer pylon reduces the minimum required available thrust, allowing a more efficient propeller for cruise, at the cost of a higher structural complexity. By using the ACAI method and altering the CG locations, maximum available thrust per rotor, and wing-mounted, inward-propellers' locations, a pylon size can be determined that is comprehensive for all the design boundaries.

C. Power

A fuel cell and battery are required to provide power to the electric motors and other electric systems of the aircraft. The battery pack is required since the power density of the fuel cell is limited and would not be able to satisfy the power demands for VTOL operations. Additionally, fuel cells are unable to throttle adequately, thus the batteries can assist the fuel cell during rapid power varying operations, such as active control or maneuvering.

Sizing the power system requires four major subsystems: air-processing, battery, fuel cell, and hydrogen storage. The fuel cell is sized with an off-the-shelf component, specifically the P-stack from Power Cell *. While this is not optimal, it ensures a conservative and realistic sizing method. The amount of stacks required is based on the power

*Accessed 4th of November, `https://powercellgroup.com/product/p-stack/`

requirement resulting in Equation 7. Let P_{cr} be the power during cruise, P_{Pstack} the maximum rating of the Powercell Pstack and M_{Pstack} the mass of a singular Powercell Pstack. Other relevant parameters for the fuel such as volume can be deduced in the same manner.

$$M_{fc} = ceil\left(\frac{P_{cr}}{P_{Pstack}}\right) \cdot M_{Pstack} \tag{7}$$

$$M_{bat} = \frac{P_{max} - P_{fc}}{P_{sp,bat}} \tag{8}$$

Concerning the battery, a trade off is performed in [4] to decide on the type of battery. Lithium-ion is chosen above more favourable options, such as solid state batteries, which have been considered but have a too low Technology Readiness Level (TRL). Ionblox Launch batteries[†] are an optimal choice due to their high power output, critical for hovering, take-off, and landing phases. Notably, these batteries are utilized in the Lilium design, enhancing the credibility of the battery figures. Characteristics of the Ionblox battery can be found in Table 4 sourced from the product datasheet [18]. Using the power density, the mass can then be easily estimated using Equation 8. The batteries are placed in in the floor structure of the cockpit, as it is favourable for the centre of gravity of the aircraft.

One of the more crucial system towards ensuring crashworthiness are the hydrogen tanks. There are two viable options for hydrogen tanks suitable for this design: Type III and Type IV. While both can handle the required 350 bars of pressure, Type IV tanks, constructed with carbon fiber and a polymer-based liner, offer superior gravimetric energy density and cost-efficiency [19].

Type IV tanks, employing composite materials, are notably lighter compared to Type III's metal construction, aligning well with vehicle applications prioritizing lower mass. These tanks support pressures up to 700 bars, exceeding the required 350 bars. [19].

Discussions with a Fuel Cell engineer at ZeroAvia [‡] indicated a Type IV tank's gravimetric energy density ranges between 7-9 wt.% hydrogen[19]. Factoring in a 20% contingency margin, a design gravimetric density of 5.4 wt.% hydrogen is established. This value represents the hydrogen mass stored relative to the total tank mass, accounting for the tank's efficiency and the fuel cell's efficiency (55%). An alternative source validates that the objective value is common in similar applications[20].

Additionally, Department of Energy (DOE) suggests a system volume of 0.6 kWh/L for a 350-bar compressed hydrogen tank [21]. Utilizing this value, the calculated system volume of the tank is significantly greater than the volume strictly required by the hydrogen, illustrating the difference for the tank's volume excluding hydrogen storage and pressure valves.

Table 4 All relevant densities and constants used in the sizing of the power system

Parameter	Value	Parameter	Value
$E_{bat,sp}$ Wh/kg	340	$P_{bat,sp}$ W/kg	3800
$E_{tank,sp}$ Wh/kg	1800	P_{Pstack} Kw	125
M_{Pstack} kg	42		

Both the battery and the fuel cell require cooling. The decision is made to only model the heat exchangers and not the tubing itself, as the topology optimization would add too much complexity. The placement of the radiators is performed post-optimization. This is done, as placement is a complicated process, whilst its influence during the optimization is irrelevant. The method used to model the heat exchanger is the $\epsilon - NTU$ method [22]. The full method is described in [5] and the implementation can be seen in [23].

Finally, additional weight from other auxiliary components such as humidifier, water separator, compressor, intercooler and turbine are also taken into account and have a combined weight of 40 kg and volume of 80 L.

D. Propulsion

In Urban Air Mobility the most challenging aspect of the propulsion system is the off-design conditions created by the vertical hover configuration. Designing a propeller capable of efficiently operating in both cruise and hover poses a considerable challenge. The objective is to optimize for cruise conditions while ensuring the propeller can meet the demands of hovering.

[†]Accessed May 30th 2023, `https://www.ionblox.com/air`

[‡]P. de Boer, Fuel cell Engineer at ZeroAvia. Technical Meeting

Before starting the optimization of the blade geometry an airfoil had to be chosen. A tradeoff is performed in [5], the result being the Wortmann FX 63-137 as shown in Figure 3. To optimize the blade geometry for cruise configuration, the method by Adkins and Liebeck is used. The method is elaborately described and supported in [24]. However, for the sake of completeness the main procedure is repeated.

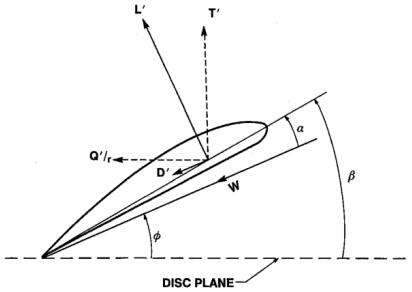

Fig. 2 Blade cross section shown with the relevant forces and angles.

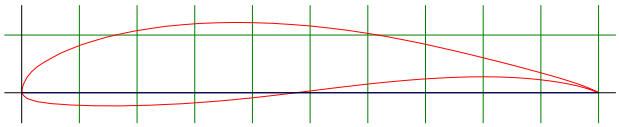

Fig. 3 The Wortmann FX 63-137 airfoil chosen for the design of the propeller

The Adkins and Liebeck design procedure starts with specified conditions including thrust, hub and tip radius, rotational rate, freestream velocity, number of blades, and a finite number of stations where blade geometry is determined. Additionally, the design lift coefficient—specific to each station if not constant—needs to be specified. The design then follows the steps below. A visual illustration of some of the parameters mentioned are depicted in Figure 2.

1) Select an initial estimate for ζ, the displacement velocity ratio ($\zeta = 0$ will work).
2) Determine the values for F, the Prandtl momentum loss factor, and ϕ, the flow angle, at each blade station.
3) Determine the product Wc, the local velocity multiplied by the local chord. Additionally compute the Reynolds number.
4) Determine ϵ, the drag-to-lift ratio, and α, the angle of attack, from airfoil section data.
5) If ϵ is to be minimized, change C_l, and repeat Steps 3 and 4 until this is accomplished at each station.
6) Determine α and α', the axial and rotational interference factor, respectively.
7) Compute the chord from Step 3, and the blade twist $\beta = \alpha + \phi$.
8) Determine the four derivatives in I and J, and numerically integrate these from the non-dimensional hub radius, ξ_0 to the non-dimensional radius $\xi = 1$.
9) Determine ζ and T_c, the thrust coefficient.
10) If this new value for ζ is not sufficiently close to the old one (e.g., within 0.1%), start over at step 2 using the new ζ.
11) Determine propeller efficiency as $\eta = \frac{T}{P_c}$, and other features such as solidity.

The equations required for executing these steps are specified in [24]. The above steps converge rapidly, rarely taking more than a few cycles, the end results being the new blade geometry.

As specified before, the following procedure only allows to optimize for a single thrust setting. Therefore, to meet off-design conditions such as hover, a check is implemented such that it is certain that this thrust setting can be met. The method for analysing an arbitrary design at any thrust setting is described in the same paper from Adkins and Liebeck; however, it is left out for brevity's sake.

If the off-design condition cannot be met, the optimization procedure restarts with an increased initial thrust setting for which the geometry is optimized. This is repeated until the off-design condition is met.

E. Structures

Designing crashworthy aviation for hydrogen-powered UAM vehicles is complex due to VTOL technology and hydrogen's volatility. Damage to the tank from fuselage deformation during a crash may cause hydrogen leakage, leading to potential fires or explosions. To ensure crashworthiness, the preliminary UAM design must thus include a deformable crash volume. This early consideration is crucial due to hydrogen's low volumetric energy density. Applying a crashed diameter coefficient (β) [25] in a preliminary design phase prevents later delays caused by large design changes. This

coefficient relates the fuselage diameter (D_{fus}) to the maximum safe crashed diameter. Since the Aetheria design features a rectangular-like cross-section, it is not feasible to directly apply the concept of a crashed diameter coefficient β. Therefore, the concept of β is adapted based on the cross-sectional area of the fuselage as shown in Equation 9.

$$\beta^2 = \frac{A_{crashed}}{A_{fuselage}} \tag{9}$$

$$AR_f = \frac{b}{h} \tag{10}$$

where β^2 now related to the crashed area instead of directly relating to the crashed diameter. The dimensions of width and height are employed in modeling the tail-cone, which is represented as a polyhedron, as depicted in Figure 4. It is important to note that this representation takes a conservative approach, considering the actual curvature of the tail would increase the vertical crumple zone further. The fuselage aspect ratio of the tail-cone undergoes a linear variation along its length. Initially, the fuselage aspect ratio is determined by the cross-section of the cabin. Towards the end of the tail, it becomes a variable that undergoes optimization to minimize fuselage length.

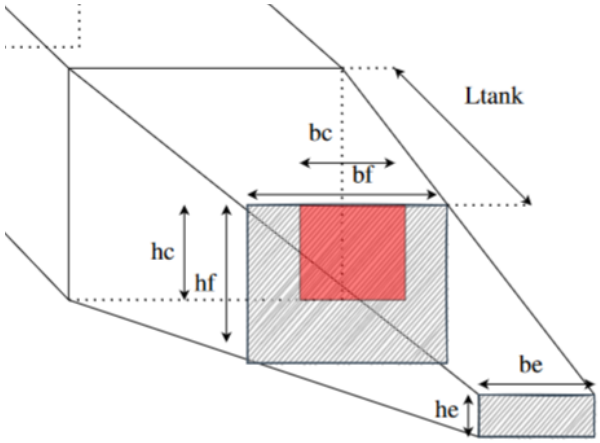

Fig. 4 Cross sectional visualization of how the the crashed diameter coefficient translates to a cross sectional fuselage.

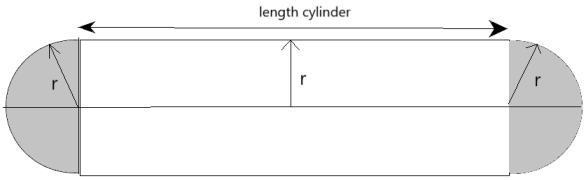

Fig. 5 Visualisation of the tank geometry

The location of storage of the hydrogen tanks can be seen in Figure 4. With a selected β of 0.5, it ensures that the hydrogen tank is not penetrated or crushed in a survivable emergency landing. Finally, the hydrogen tank is modeled as shown in Figure 5, a cylinder with length l_{cyl} and two half spheres that have a radius equal to that of the cylinder. Using this model the following steps are used to obtain the limiting fuselage length:

1) Define a L_{tank} and calculate the tank radius from the required hydrogen volume. There are two tanks, so the volume per tank is half the total volume. The volume can be computed by finding the roots of the equation as shown in Equation 11.

$$\begin{aligned} V &= \pi r^2 l_{cyl} + \frac{4}{3}\pi r^3 \\ l_{cyl} &= l_{tank} - 2r \\ -\frac{2}{3}\pi r^3 + \pi l_{tot} r^2 - V &= 0 \end{aligned} \tag{11}$$

2) From the radius of the tank, the minimal required crash cross-section can be obtained by considering that two tanks have to fit side by side. Consequently, the width of the crash area has to be at least 4 times the radius, thus leading to the simple equation Equation 12:

$$b_c = 4r \tag{12}$$

3) The tail-cone cross-sectional area at the end of the hydrogen tanks can be obtained by combining Equation 9 and Equation 10, the result being Equation 13:

$$A_f = \frac{b_c^2}{AR_f \cdot \beta^2} \tag{13}$$

where AR_f is the aspect ratio of the fuselage at the limiting cross-section. Which is determined by the length of the hydrogen tank, AR_{cabin} and AR_e. It is crucial to note however that AR_f is not known and no explicit solution exists as it is dependent on the tail-cone length. Hence, an initial estimate is made on the aspect ratio from which a tail-cone length can be computed. This new tail-cone length is then used to compute an updated aspect ratio. This is repeated until an error lower than 0.5% is achieved between AR_{f_i} and $AR_{f_{i+1}}$. Please reference Figure 4 for a spatial illustration of the problem.

4) The tail-cone length can then be obtained using similar triangles leading to the equation shown in Equation 14. The assumption is that the cross-sectional surface area at the end of the tail-cone approaches zero.

$$l_{tail} = \frac{h_0}{h_0 - h_f} l_{tank} \tag{14}$$

This process is iterated for a range of L_{tank} values to find the minimal tail-cone length. Thus, a formal expression of the optimization is shown in Equation 15:

$$\begin{aligned} &\textit{Minimize: } l_{tail}(AR_e, l_{tank}, V) \\ &\textit{subject to: } 4 \cdot r(V) < b_c(AR_e, l_{tank}) \\ &\qquad\qquad 2 \cdot r(V) < h_c(AR_e, l_{tank}) \end{aligned} \tag{15}$$

In this optimization the volume V is a variable imposed by the influence of several other departments and hence can not be varied. However, the length of the tank and the aspect ratio at the end of the tail AR_e can be chosen such that the length of the tail is minimized.

To determine the weight of critical structures like the fuselage, wing, and tail, Class II weight estimations are employed. Specifically, the Cessna method from [26] is utilized, and occasionally the Torenbeek method. Both methodologies are tailored for General Aviation aircraft and are chosen based on their proximity to our design objectives. For a condensed overview, please refer to Table 5, while the full implementation can be found in the source code made available with the present study [23].

Table 5 Utilization of Class II weight estimations for diverse components.

Component	Equations	Method
Wing	$0.04674 w_{to}^{0.397} S^{0.36} n^{0.397} A^{1.712}$	Cessna
Fuselage High wing	$14.86\ w_{to}^{0.144} \left(\frac{l_f}{\Phi_f}\right)^{0.778} l_f^{0.383} n_{pax}^{0.455}$	Cessna
Landing gear	$0.04 w_{to} + 6.2$	Cessna
Horizontal Tail	$\frac{3.184 w_{to}^{0.887} S_h^{0.101} A_h^{0.138}}{174.04 t_{r_h}^{0.223}}$	Cessna
Nacelles	$0.24 P_{max}$	Cessna
Flight Control System	$0.0168 w_{to}$	Cessna
Electrical system	$0.0268 w_{to}$	Cessna
Instrumentation & Avionics	$0.008 w_{to} + 40$	Torenbeek
Air conditioning	$0.018 w_{to}$	Torenbeek
Furnishing	$0.412 n_{pax}^{1.145} w_{to}^{0.489}$	Cessna

V. MADO problem formulation

All system models from the multiple disciplines that were previously described have been implemented in the Python package Aetheria [23]. To address the integration of subsystems and consider crashworthiness within volume

constraints, a double-loop multidisciplinary design optimization is employed. The inner loop ensures design convergence by handling feedback mechanisms present in the design procedure, while the outer loop focuses on minimizing the mission energy through the aspect ratio of the main wing. A design is only passed to the outer loop once a converged design has been reached in the inner loop. This is achieved when there is a 0.5% difference in the MTOM of the current and previous iteration with a limit of 10 iterations. A visual representation of the complete MADO in the form of an N2 chart is shown in Figure 6.

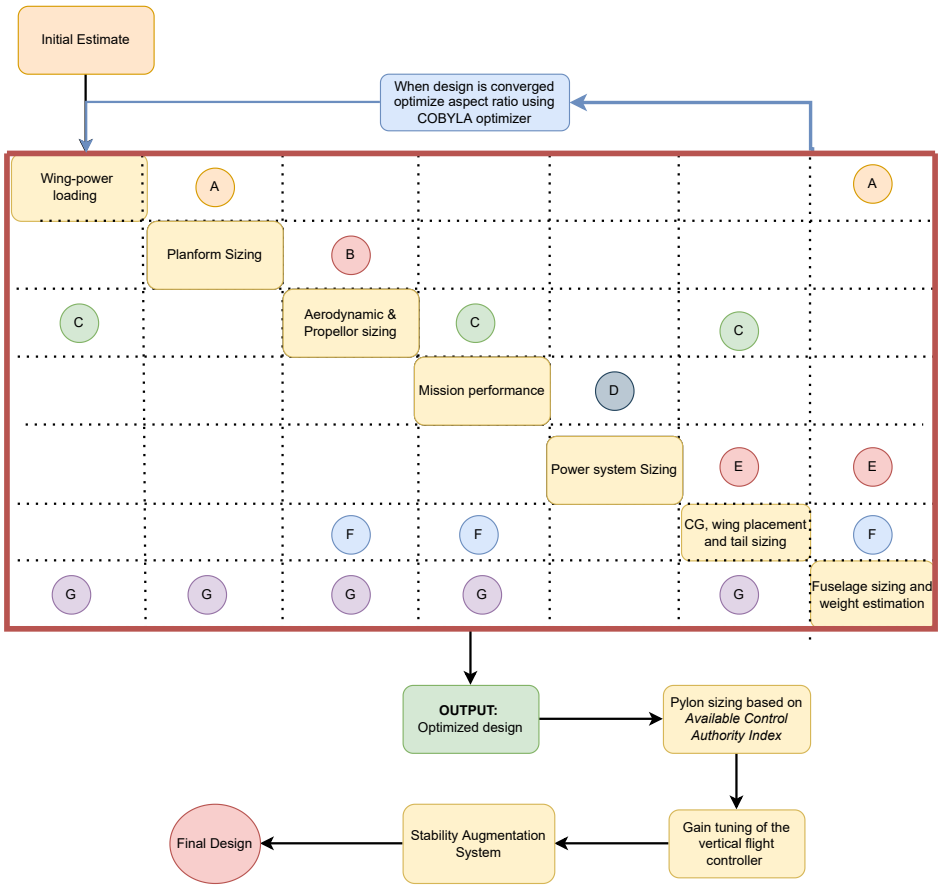

Fig. 6 N2 chart of the MADO showing the double loop implementation and design steps taken after an optimized design has been reached.

To ensure the clarity of Figure 6, concise labels sourced from Table 6 have been utilized. The MADO commences with an initial estimate, comprehensively detailed in Table 7, essential for initializing the procedure. The majority of parameters listed in Table 7 serve as initialization values and possess little to no impact on the optimization process. Notably, only the maximum takeoff weight and aspect ratio of the main wing wield significant influence over the optimization procedure. Further insights on this aspect are elaborated upon in section VII.

Table 6 Description of labels shown in Figure 6

A	B	C	D	E	F	G
W/S	S	C_{D_0}	$E_{mission}$	V_{tank}	CG_{oem}	l_f
n_{max}	b	C_{L_α}	P_{max}	M_{fc}	CG_{min}, CG_{max}	$MTOM$
$C_{L_{cr}}$	C_{root}	L/D	$t_{mission}$	M_{bat}	$C_{L_{h,cr}}$	M_{wing}
n_{ult}	C_{tip}	e	T_{max}	M_{rad}	S_H	M_{vtail}
	C_{mac}	$\frac{d\epsilon}{d\alpha}$		V_{fc}	$\frac{S_h}{S}$	$M_{fuselage}$
	Λ_{le}	η_{prop}		V_{bat}	Γ	
		$C_{L_{endur}}$		M_{tank}		

Table 7 Initial estimate

Parameters		
AR	M_{misc}	C_{L_α}
M_{wing}	$M_{cooling}$	η_{prop}
e	Glide Slope	$C_{L_{max}}$
S	l_{tail}	$C_{m_{ac}}$
$\Lambda_{c/4}$	Upsweep	C_{d_0}
l_{w-h}	l_{tank}	M_{fuse}
M_{tail}	M_{lg}	OEM
AR_h	MTOM	l_{fuse}

Following the initial estimate, a design point is selected based on wing- and power- loading, constituting the initial step outlined in subsection IV.A. This chosen design point then drives the planform sizing, subsequently influencing aerodynamic and propeller sizing. Once the planform, propulsion, and aerodynamics are modeled, performance estimates for a fixed mission (as detailed in subsection IV.A) become feasible. Leveraging the resulting power and energy figures, mass and volume sizing for the powertrain is conducted. This mass and volume become pivotal in the subsequent subsystem, where the computation of the center of gravity takes place, the optimal wing location is determined, and the sizing of the V-tail is executed.

At this stage in the MADO, the aircraft's design is nearly finalized, with particular attention turned towards ensuring crashworthiness, especially in relation to the hydrogen tanks. The sizing of these tanks is contingent upon the available volume within the tail-cone. As detailed in subsection IV.E, a model is employed to determine the length of the tail-cone, subsequently influencing the overall fuselage length. This method guarantees an adequate and crashworthy volume within the aircraft, prioritizing safety considerations. With the design fully defined, the class II weight estimations are used to define the remaining weights of the aircraft.

Evident from Figure 6 is that the final subsystem, the fuselage sizing, affects most preceding subsystems and is therefore the main source of feedback in the system. It is for this reason that the $MTOM$ has been chosen as the parameter on which the convergence metric is based.

Moreover, as depicted in Figure 6, the design generated by the MADO necessitates further processing, specifically involving the adjustment of pylon sizing and design of a vertical flight controller, as it is an inherently unstable phase. The reasoning behind these actions is elaborated upon in subsection IV.B.

Employing the MADO framework, the formal representation of the optimization process is depicted in expression (16). The optimization is executed using COBYLA (Constrained Optimization by Linear Approximation) as the chosen optimizer. COBYLA proved most effective for straightforward optimizations involving a single variable. Given the intricate nature of the multidisciplinary analysis, optimizers reliant on gradients are deliberately avoided in the present study, given their tendency to converge towards the first local minimum.

$$
\begin{aligned}
\min_{\text{AR}} \quad & E(\text{AR}, \mathbf{x}) \\
\text{where} \quad & \boldsymbol{x} = [M_{misc}, C_{L_\alpha} \cdots l_{fuse}] \quad \text{(Table 7)} \\
\text{with bounds} \quad & 5 \leq A \leq 15 \\
\\
\text{subject to} \quad & MTOM \leq 3175 \\
& 7.4 \leq b \leq 14 \\
& l_{fuse} \leq 14
\end{aligned}
\tag{16}
$$

The maximum takeoff Mass constraint in expression (16) ensures compliance with the Special Condition for VTOL as specified in [3]. Furthermore, maintaining fuselage dimensions and a wingspan below 14 meters is important for enabling landing on helipads, a critical capability for Urban Air Mobility operations.

VI. Results

The proposed MADO methodology is executed using an initial estimate of 2500kg for the MTOM and 9.4 for the aspect ratio. The resulting design parameters are detailed in Table 8. Note that subscripts marked with the letter h signify properties related to the aircraft's tail.

Table 8 The key parameter defining the resultant design upon executing the MADO with an initial estimate of an MTOM of 2500 [kg] and an aspect ratio of 9.4.

Parameter	Value	Parameter	Value	Parameter	Value
b	12.3 [m]	$MTOM$	3097 [kg]	cg_{fr}	5.4 [m]
A	9.4 [-]	l_{fuse}	11.75 [m]	cg_{rear}	6.2 [m]
A_h	5 [-]	h_{fuse}	2 [m]	wing $l_{c_{1/4}}$	5.76 [m]
Γ_h	26°	w_{fuse}	2.2 [m]	e	0.77 [-]
Λ_{LE}	2.31° [-]	l_{tank}	3.2 [m]	$C_{L_{cr}}$	0.56 [-]
S	16.12 [m^2]	r_{tank}	0.227 [m]	C_{d_0}	0.028 [-]
S_h	6.7 [m^2]	V_{tank}	1.13 [m^2]	$C_{d_{ind}}$	0.014 [-]
b_h	5.8 [m^2]	η_{prop}	84%	$\frac{L}{D}_{cr}$	13.3 [-]
P_{max}	1007 [kW]	E_{tot}	320 [kWh]	$C_{L_{max}}$	1.6 [-]

An isometric and three view drawing of the design is provided in Figure 7. Notably, the front rotors are no longer attached to the wing via a pylon but are now connected to the fuselage. The reasoning behind this choice will be explored in section VII. Furthermore, note that the design is more voluminous and relatively heavier than typical eVTOLs currently being developed e.g Lillium, Joby or Archer.

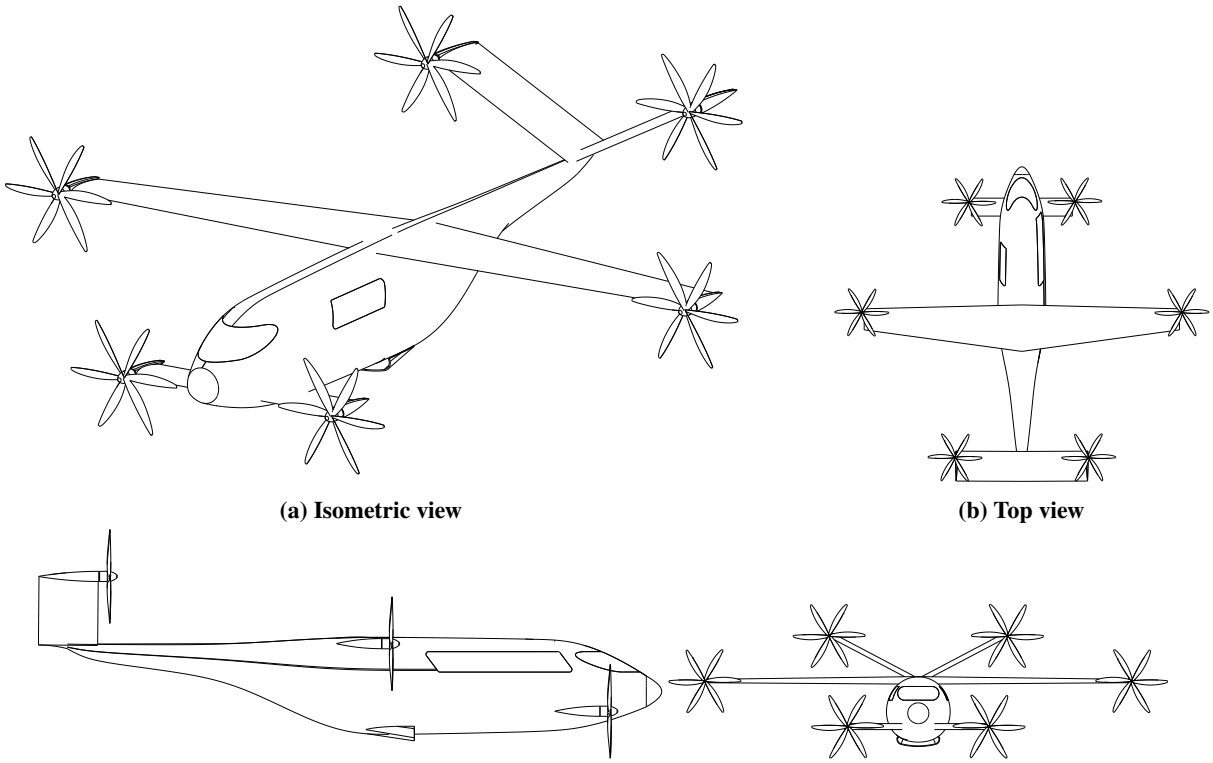

(a) Isometric view **(b) Top view**

(c) Side view **(d) Front view**

Fig. 7 Three-view drawing depicting the design derived from the MADO execution.

The internal volume of the fuselage is compartmentalized, as shown in Figure 8, to accommodate all components while ensuring a crashworthy area beneath the hydrogen tanks. Positioned directly aft of the firewall, marking the boundary between the cabin and tail-cone, is the fuel cell. In addition to the fuel cell, various auxiliary equipment such as the compressor and humidifier are situated within. The tank, spanning a total length of 3.2m, is placed in the upper section of the tail-cone. Importantly, the space below the tank must not contain rigid objects or structures that could potentially puncture the tank in the event of a crash.

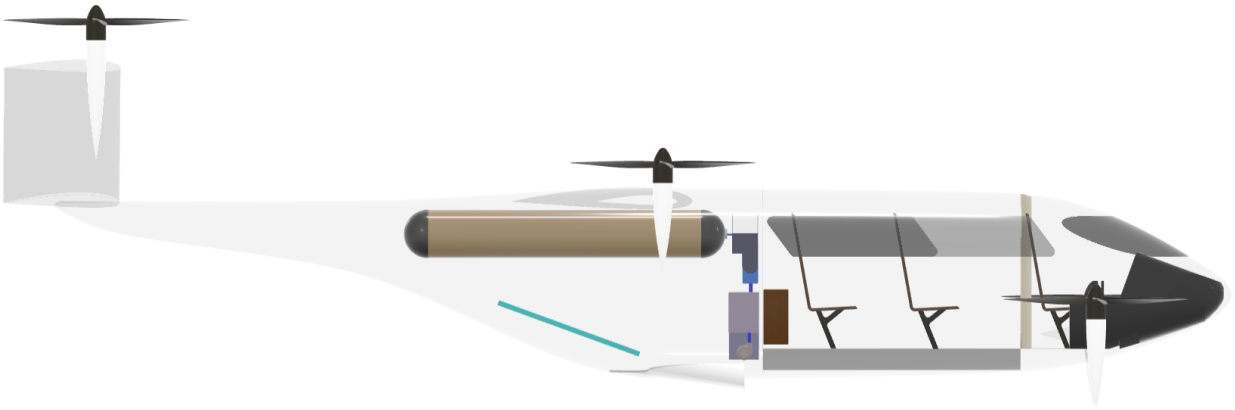

Fig. 8 Side view of the orientation of the internal components of the aircraft.

All the components in the aircraft result in a weight and energy distribution of the various phases as outlined in Figure 9 and Figure 10. The miscellaneous component in the weight distribution includes the flight control system, electrical system, instrumentation & avionics, air conditioning and furnishing.

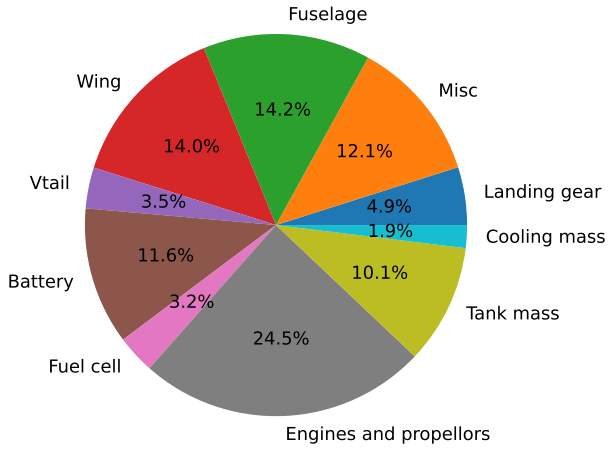

Fig. 9 The weight distribution of the resulting design from the MADO problem formulation.

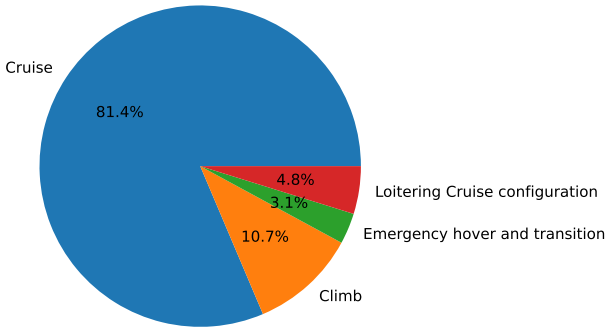

Fig. 10 The energy distribution of the resulting design from the MADO problem formulation.

Crucial insights into the internal drivers of the MADO often reside within the convergence history of its most influential parameters. As showcased in Figure 11, the convergence history of the MADO is presented for four key parameters: aspect ratio, maximum takeoff mass (MTOM), fuselage length (l_{fuse}), and mission energy. The horizontal axis represents the number of iterations from the initiation of the MADO process. Each iteration being a complete traversal through the N2 chart, as illustrated in Figure 6. On the vertical axis, the values of the respective parameters are depicted, with caution advised regarding the varying scales utilized in each graph. It is important to note that the initial estimate of MTOM, as mentioned at the section's outset, does not commence at the stated value due to the first sample being taken after completing a full iteration.

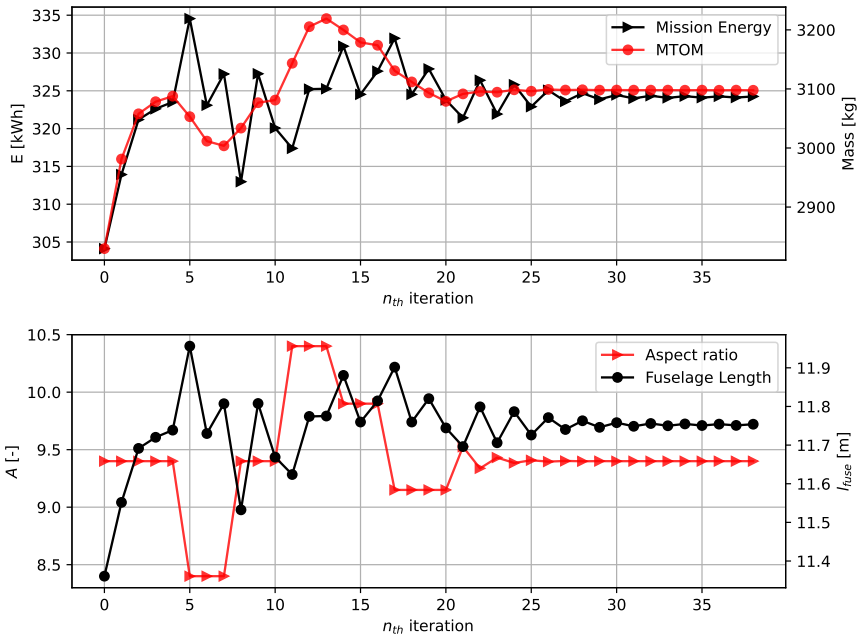

Fig. 11 Evolution of four key parameters in the MADO Convergence History. The horizontal axis depicts the number of iterations, while the vertical axis represents each parameter's values.

VII. Discussion

The objective of this paper is to evaluate the viability of a long-range vehicle powered by hydrogen, with a specific focus on crashworthiness considerations. The design process is undertaken through a comprehensive Multidisciplinary Analysis and Design Optimization (MADO), visually represented in Figure 6. Additionally, an effort is made to uncover the internal driving parameters and relationships among the various subsystems in a long-range hydrogen powered eVTOL.

As anticipated, the design faces significant volume constraints, resulting in an elongated fuselage measuring 11.75 meters, detailed in Figure 7. This elongation stems from the considerable length of each of the two tanks, spanning 3.2 meters each, accompanied by the crashworthy volume surrounding the tanks. However, the tail-cone, spanning a total of 6.6 meters, is elongated more than required due to the modeling assumption of a polyhedral shape. A more upswept tail near the end of the fuselage would have shortened the current length.

However, shortening the fuselage would have led to an oversized v-tail, given that the existing tail surface already covers an area 42% that of the wing. The substantial gap needed between the tail and wing is a consequence of the considerable shift in the center of gravity, prompted by the spacious seating arrangement and generous luggage capacity.

This observation, coupled with the potential for more upswept and shorter fuselage, suggests at the possibility of enhancing performance through a sophisticated and optimized tail-cone topology. A visual illustration of what this would look like is already shown in Figure 7. However the numerical implications have been left as a recommendation.

Additionally, the elongated fuselage and specific tail placement demanded a reassessment of the aircraft's vertical flight stability. To ensure vertical controllability, the aircraft's center of gravity must be approximately aligned with the center of the six rotors to minimize variations in thrust levels. Adhering to the baseline configuration detailed in section III would have rendered unfeasible pylon lengths. Consequently, a decision is made to affix the front rotors to the fuselage via a pylon. After considering various alternatives, this solution is chosen for its lower impact on noise pollution, making it the preferred option. The attachment of the engines to the fuselage induce extra loads on the fuselage that would require higher fidelity weight estimations for the fuselage structures, a recommendation left for next design iterations.

Shifting focus from stability considerations, it is clear that the substantial surface area of the fuselage and the added weight from the tank, batteries, and auxiliary systems contribute to a heavier design. Figure 9 details the distribution of this weight. While engines and propellers constitute the bulk of the weight, the batteries still hold a considerable share,

despite hydrogen being our primary energy source. This is attributed to the exceedingly high power demand during take-off, which drives the battery sizing.

Nevertheless, a fully electric aircraft would likely not be able support as much energy without exceeding the weight limits imposed by EASA. Thanks to the scalability enabled by hydrogen, fully electric eVTOLs are rapidly a less suitable option when it comes to long range eVTOLs, as the low energy density batteries would increase the weight exponentially. Figure 10 confirms that the great majority of the energy is consumed in the cruising phase. Since cruise is a high energy and low power demanding phase, hydrogen and its high energy density can deliver the needs of a longer flight with a large potential to be scalable for larger ranges.

A. Sensitivity

The selection of the crash diameter and tail cone aspect ratio has proven to significantly affect the overall design. Consequently, a sensitivity analysis is conducted on both parameters to visualize potential design alterations. As depicted in Figure 12, the sensitivity analysis on the ending aspect ratio of the fuselage indicates possibilities for further optimization. It suggests that enhancing the fuselage's width towards the rear could contribute to design refinements, by reducing the tailcone length by approximately half a meter.

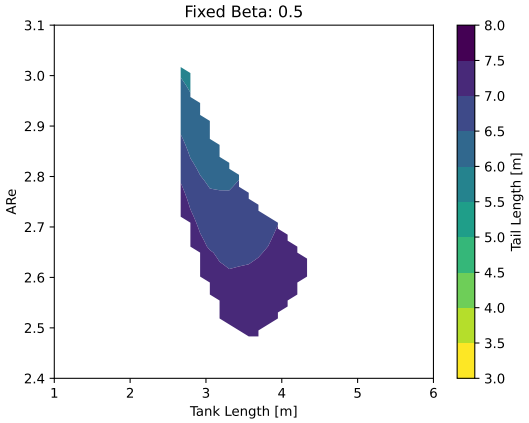

Fig. 12 Sensitivity of the ending aspect ratio of the fuselage for a fixed crashed diameter coefficient of 0.5.

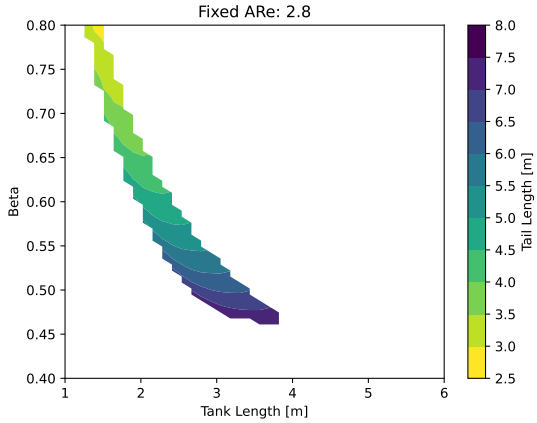

Fig. 13 Sensitivity of the crashed diameter coefficient for a fixed ending aspect ratio of the fuselage of 2.8.

The sensitivity analysis depicted in Figure 13 illustrates the impact of the crashed diameter coefficient. This parameter emerges as notably more influential than the ending aspect ratio of the fuselage. Relaxing the constraint on the crashed diameter could potentially reduce the fuselage length by up to 3 meters. However, surpassing a crashed diameter coefficient of 0.6 might pose significant challenges. Hence, it becomes evident that the assumed conservative value of 0.5 used in the present study enhances the feasibility of the eVTOL design.

B. Comparative Review

The output of this optimisation procedure can be validated through comparison with current existing projects. Since the design of those projects and the output of this optimisation may have different characteristics, this comparison is largely based on engineering judgement. The two analysed cases are *Joby S4*[§] and *Vertical Aerospace VX4*[¶], because of the design similitude.

The *Joby S4* VTOL aircraft is similar to *Aetheria*, in that it consists on a tilt-rotor aircraft, comprising of 6 rotors, with a payload capacity of 4 passengers. This aircraft is considerably smaller in most dimensions than the optimisation output. The main focus of comparison is the relatively short distance between the wing and the tail, as well as the fact that the inner-most, foremost propellers are attached to the wing via extended pylons. Regarding the first point, it is believed that because of the smaller cabin design of the *Joby S4*, the static loading diagram yields a low variation of the

[§]Accessed 2nd of December, `https://www.jobyaviation.com/`

[¶]Accessed 2nd of December, `https://vertical-aerospace.com/`

CG. This would, in turn, relieve the pitch moments of the aircraft, making a long tail-cone or tail-boom unnecessary. Moreover, the smaller design configuration, allows for relatively small extended pylons to be wing-mounted to support the inner-most, foremost propellers. In the *Aetheria* design, given its larger size, it is preferable to have these mounted on the fuselage.

The *Vertical Aerospace VX4* is a lift-and-cruise aircraft, with dimensions closer to those of *Aetheria*. The long tail-boom implemented in the design of the *VX4*, showcases the stability and control difficulties that most similar projects are facing. Similarly, the optimisation output by using the described method under the given constraints, has yielded a relatively long aircraft, at 11.75m, compared to *VX4*'s 13m. Because of the hydrogen tanks and crashworthiness considerations, the tail-boom option was not explored in this scenario as a large fuselage volume is required at the tail. However, a tail-boom could be envisioned at the aft-most part of the fuselage, behind the hydrogen storage. For illustrative purposes, this is displayed in Figure 7, although it is not implemented in the MADO formulation.

By examining the previous two examples, it is deduced that on the larger scale, the MADO outputs are consistent with trends and results of products with similar characteristics. This can be used preliminarily as a validation method for the feasibility and reliability of the used methodology.

VIII. Conclusion

As the results show, designing a hydrogen powered eVTOL aircraft whilst considering crashworthiness in a preliminary stage proves to be a challenging but feasible endeavour. The main challenges herein encountered concerned the large volume required for hydrogen, the aerodynamic penalty of this extra volume, and the intricate design trade-off between the length of the fuselage and the horizontal-vertical stability.

The large volume required for the hydrogen tanks while considering crashworthiness was attested to by utilizing this volume as the main driver for the fuselage size. It is then of great importance in the MADO framework that the fuselage dimensions are coupled with the effected subsystem such as aerodynamics and stability.

Additionally, the design suffers from a weight penalty due to the auxiliary equipment necessary for operating a hydrogen-powered aircraft. Bringing the final design to a weight of 3000 kg, nearing the certification limit. Despite this, hydrogen-powered UAM (Urban Air Mobility) vehicles exhibit promise in the long-range market. Their good scalability and superior energy carrying capacity outperform those of fully electric eVTOLs, positioning them as contenders in this domain.

A. Recommendations

Future recommendations can be categorised in the following: depth of optimisation, speed improvements, and fidelity of the used models.

The current design change of attaching the front rotors to the fuselage is not properly modeled in the MADO as it was applied post MADO. In future iterations its effect on the structural weight and stability should be taken into account.

Additionally, the fidelity of the results can be improved by including deeper aerodynamic analyses on the product design. The two most relevant solutions can be derived from propeller-wing interactions, and by applying a higher-fidelity model for aerodynamics, including an estimation for $C_{L,max}$.

Moreover, the tail-cone is currently modelled as a polyhedron during the MADO, which as discussed in section VII is not optimal due to the combination of volume and stability constraints. A revised tail-cone design approach has been shown however has not been taken into account numerically. Doing so, would likely improve the current design.

Finally, regarding computational efficiency for the MADO, the current implementation of methods involving the ACAI method can be revised. The pylon sizing and vertical flight CG range determination are based on repetitive loops, that mostly return non-useful data. By optimising these functions, the optimiser can see large improvements in performance.

Acknowledgements

We would like to thank S.G.P Castro, F. Scarano, J. Benad and M.B. Lopez for their unwavering support during both the initial start of the project and the conference paper that followed.

Furthermore, we would like to give special thanks to the team members who were part of the initial project: B.A. van Battum, L. Middendrop, C. Karaca, W. Albers, S. de Rijke and E. Hadzhiyski.

Finally, we would like to thank Delft University of technology for making the presentation at SciTech 2024 possible.

References

[1] World Nuclear Association, "Heat Values of Various Fuels - World Nuclear Association," , September 2016. URL https://www.world-nuclear.org/information-library/facts-and-figures/heat-values-of-various-fuels.aspx, accessed on November 16, 2023.

[2] Albers, W., Arends, J., van Battum, B. A., Hadzhiyski, E., Karaca, C., Keijzer, D. M., Middendorp, L., de Rijke, S., Sarıgöl, B., and Simon Soria, C., "Baseline Report - Aetheria, hydrogen-based long- range eVTOL designed for crashworthiness," , Jun. 2023. https://doi.org/10.5281/zenodo.8055976.

[3] EASA, "Second Publication of Means of Compliance with the Special Condition VTOL," *MOC-2 SC-VTOL*, Vol. 3, 2022, pp. 49–62. URL https://www.easa.europa.eu/en/document-library/product-certification-consultations/special-condition-vtol.

[4] Albers, W., Arends, J., van Battum, B., Hadzhiyski, E., Karaca, C., Keijzer, D. M., Middendorp, L., de Rijke, S., Sarıgöl, B., and Simon Soria, C., "Midterm Report - Aetheria, hydrogen-based long- range eVTOL designed for crashworthiness," , Jun. 2023. https://doi.org/10.5281/zenodo.8056301.

[5] Albers, W., Arends, J., van Battum, B. A., Hadzhiyski, E., Karaca, C., Keijzer, D. M., Middendorp, L., de Rijke, S., Sarıgöl, B., and Simon Soria, C., "Final Report - Aetheria, hydrogen-based long-range eVTOL designed for crashworthiness," , Jul. 2023. https://doi.org/10.5281/zenodo.8125990.

[6] DeYoung, J., and Harper, C. W., "Theoretical symmetric span loading at subsonic speeds for wings having arbitrary plan form," NACA Technical Report NACA-TR-921, National Advisory Committee for Aeronautics (NACA), 1948. URL https://ntrs.nasa.gov/archive/nasa/casi.ntrs.nasa.gov/19930091985.pdf, accession Number: 93R21275.

[7] Raymer, D. P., *Aircraft Design: A Conceptual Approach*, 6th ed., American Institute of Aeronautics and Astronautics, Reston, VA, 2018. https://doi.org/10.2514/4.104909.

[8] Beyne, E. E., and Castro, S. G., "Preliminary performance assessment of a long-range eVTOL aircraft," *AIAA SciTech Forum*, 2022. https://doi.org/10.2514/6.2022-1030.

[9] Anderson, J. D., *Introduction to Flight*, 6th ed., McGraw-Hill, 2008.

[10] Roskam, J., *Airplane Design, Part II : Preliminary Configuration Design and Integration of the Propulsion System*, Roskam Aviation and Engineering Corporation, Ottowa, Kansas, 2018.

[11] EASA, "Certification Specifications for Normal Category Aeroplanes (CS-23)," , 2023. URL https://www.easa.europa.eu/en/document-library/certification-specifications/group/cs-23-normal-utility-aerobatic-and-commuter-aeroplanes.

[12] Roth, B., "Control Power Design Requirements for Aircraft Flying Qualities," , 2009. URL https://engineering.purdue.edu/~andrisan/Courses/AAE451_F2009/Buffer/Control_Power/flying_qualities_doc_05012009.pdf.

[13] Alba-Maestre, J., Beyne, E., Buszek, M., Cuadrat-Grzybowski, M., López, N. S., Poliakov, N., Prud'homme van Reine, K., Santamaría, A. M., Schoser, J., and Wadia, K., "Midterm Report - Multi-Disciplinary Design and Optimisation of a Long-Range eVTOL Aircraft," , Nov. 2021. https://doi.org/10.5281/zenodo.5720244.

[14] Paul E. Pursee, J. P. C., "Experimental verification of a simplified vee-tail theory and analysis of available data on complete models with vee tails," , 1945. URL https://ntrs.nasa.gov/citations/19930091901.

[15] Drela, M., *Flight Vehicle Aerodynamics*, The MIT Press, Cambridge, Massachusets, 2014.

[16] Du, G.-X., Quan, Q., Yang, B., and Cai, K.-Y., "Controllability Analysis for Multirotor Helicopter Rotor Degradation and Failure," *Journal of Guidance Control and Dynamics*, Vol. 38, 2015. https://doi.org/10.2514/1.G000731.

[17] EASA, "Certification Specifications, Acceptable Means of Compliance and Guidance Material for Small Rotorcraft (CS-27)," , 2023. URL https://www.easa.europa.eu/en/document-library/certification-specifications/group/cs-27-small-rotorcraft.

[18] Ionblox, "Ionblox Launch (High Energy AV Cell) product sheet," Ionblox, 2023. URL https://www.ionblox.com/air, accessed 30-05-2023.

[19] Muthukumar, P., Kumar, A., Afzal, M., Bhogilla, S., Sharma, P., Parida, A., Jana, S., Kumar, E. A., Pai, R. K., and Jain, I., "Review on large-scale hydrogen storage systems for better sustainability," *International Journal of Hydrogen Energy*, 2023. https://doi.org/10.1016/j.ijhydene.2023.04.304.

[20] U.S Department of Energy (DOE), "Hydrogen Storage," *Multi-Year Research, Development, and Demonstration Plan*, 2012. URL https://www.energy.gov/sites/default/files/2015/05/f22/fcto_myrdd_storage.pdf.

[21] Department of Energy (DOE), "Energy requirements for hydrogen gas compression and liquefaction as related to vehicle storage needs," *DOE Hydrogen and Fuel Cells Program Record*, 2009. URL https://www.hydrogen.energy.gov/pdfs/9013_energy_requirements_for_hydrogen_gas_compression.pdf.

[22] *Frontmatter*, John Wiley & Sons, Ltd, 2003, pp. i–xxxii. https://doi.org/10.1002/9780470172605.fmatter.

[23] Keijzer D. et al., "Aetheria eVTOL multi-disciplinary analysis Python package (Version 2023.2)," , Nov. 2023. https://doi.org/10.5281/zenodo.10276957.

[24] Charles N. Adkins, R. H. L., "Design of Optimum Propellers," *JOURNAL OF PROPULSION AND POWER*, Vol. 10, No. 1, 1994. https://doi.org/10.2514/3.23779.

[25] Castro, S. G. P., "Research vision presented to the Faculty of Aerospace Engineering, Delft University of Technology," , 2023.

[26] Roskam, J., *Airplane Design. Pt. 5. Component Weight Estimation*, Roskam Aviation and Engineering, 1985.